ANALYSIS OF HOVER/HOVERING TURN OF A COMPLETE HELICOPTER CONFIGURATION USING A COUPLED AERODYNAMICS-FLIGHT DYNAMICS SOLVER

Se Hwan Park, Yeon Bok Chu, Sang Ha Park, Dong-Ho Seo and Duck Joo Lee
KAIST, Daejeon, Republic of Korea

Abstract

Loss of yaw control effectiveness has been a common cause of helicopter accidents. Comprehensive analysis of yawing motion and tail rotor control is necessary to reduce the helicopter crash. The authors considers that the analysis of hovering turn is an appropriate starting point as a preliminary research. In the present paper, the trimmed pilot input angle for hover flight was found using the analytic and numerical trim procedures. The pilot input obtained from the analytic trim analysis was used as an initial condition for the hover flight simulation of a complete UH-60 helicopter configuration to accelerate the convergence in the numerical rotor trim. After the hovering flight for a while, the pedal input was given for hovering turn flight simulation. The computed result was compared with the flight test data and the nonlinear analysis result with the dynamic trim. A vortex lattice/panel/vortex particle method was used for aerodynamics simulation, and the simplified flight dynamics approach was used for 1 DOF flight in yawing direction.

1. INTRODUCTION

The loss of control effectiveness causing helicopter accidents can be classified into four different types of control: yaw, vertical, roll, and pitch. Fig. 1 shows that the accident rate by the loss of yaw control is the highest, and this might be closely related with a tail rotor and an anti-torque issue. The tail rotor produces the thrust force to counterbalance the torque generated by the main rotor. In case of the helicopter control, yawing and rolling controls are coupled because of the characteristics of helicopter control mechanism. This is the reason why flying a helicopter is usually considered to be difficult and dangerous. However, the authors thought that understanding a hovering turn flight could be a good first step to analyse and reduce the helicopter accidents caused by the loss of yaw control or tail rotor problems. Even though the hovering turn looks simple, the flow physics during the hovering turn or hovering flight under crosswind is more complex and unsteady than expected. This is because the fuselage is strongly influenced by the main rotor wake as well as the transient crosswind whose magnitude also varies with the distance from the center of rotation. Also, the cross wind makes the tail rotor operate in climb or descent flight. Thus, the tail rotor could enter into vortex ring state as shown in Fig. 2 (Ref. 2). It would cause the loss of yaw control effectiveness and consequently helicopter accidents. Cress (Ref. 2) mentions that wind from either thrust side or wake side of the tail rotor and main rotor blade tip vortex ingestion at tail rotor are the reason for loss of tail rotor effectiveness. Therefore, the hovering turn is potentially a hazardous maneuver.

There has been little research on the hover turn flight except that the tail rotor could enter into the vortex ring state during the hovering turn or the hover flight in crosswind. However, coupled aerodynamics-flight dynamics analysis has been continued regarding the maneuver flight of an isolated main rotor and the forward flight of a complete helicopter configuration. Ananthan and Leishman (Ref. 3) simulated pop-up, pop-down and roll reversal maneuvers of a rotor using a free wake vortex method. Jeon (Ref. 4) used a full-span free-wake method for pop-up and pop-down flight of a rotor with inspection on tip vortex and its counter rotating trailed wake vortex. Abhishek et al. (Ref. 5-6) simulated the pull-up maneuver of an isolated main rotor with the prescribed pilot control angles and trajectory.

When it comes to a full helicopter analysis, the main rotor trim procedure was adopted in forward flight simulation using the computational fluid dynamics solvers (Ref. 7-10) and the vortex method (Ref. 11-12). Lee et al. (Ref. 13-14) simulated a hover flight of the complete UH-60 helicopter configuration using the Euler solver to investigate rotor downwash effect on free-flight rocket launched from the helicopter. A simplified trim was adopted such that the torque produced by the main rotor in compensated by the tail rotor.

The purpose of the present research is to understand the flow characteristics around a helicopter during its hover turn flight. In this paper, the authors simulate the hovering turn of a full configuration helicopter by coupling the

aerodynamic solver with a simplified flight dynamics model.

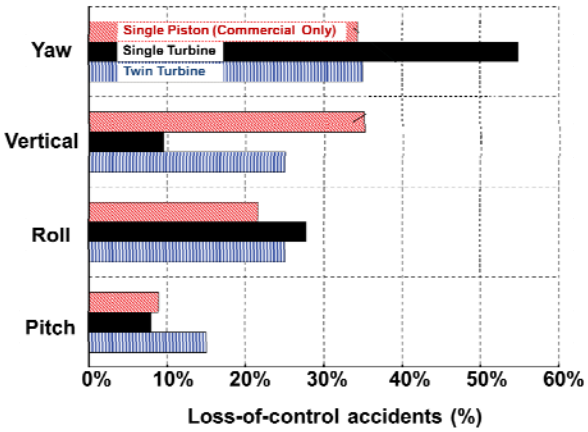

Figure 1 Helicopter accidents owing to loss of control (Ref. 1)

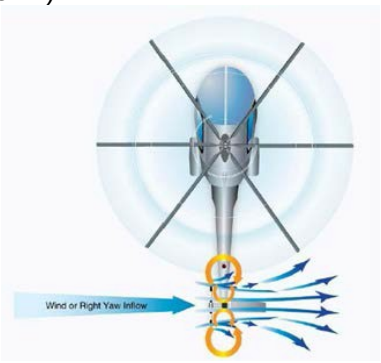

Figure 2 Tail rotor in vortex ring state with port winds (Ref. 2)

2. METHODOLOGY

2.1. Aerodynamics Model

2.1.1. Surface Pressure with Poisson Equation

The stagnation pressure increase and unsteady pressure fluctuation at the fuselage surface due to the main rotor wake should be predicted accurately. However, conventional Bernoulli equations cannot capture the stagnation pressure increase unless a special treatment is used. In the present paper, the pressure at the fuselage surface is computed using the integral solution of a Poisson equation (Ref. 11, 12, 15). The Poisson equation is

(1) $$\nabla^2 B = \nabla \cdot ((\mathbf{V}_\infty + \mathbf{v}) \times \boldsymbol{\omega})$$

where B is specific stagnation enthalpy defined by

$$B = \frac{p - p_\infty}{\rho} + \frac{1}{2}\left[(\mathbf{V}_\infty + \mathbf{v}) \cdot (\mathbf{V}_\infty + \mathbf{v}) - \mathbf{V}_\infty \cdot \mathbf{V}_\infty\right].$$

$\mathbf{V}_\infty$ and $\mathbf{v}$ are freestream velocity and perturbation velocity, respectively, and $\boldsymbol{\omega}$ is vorticity. The integral solution can be derived as

(2)

$$\beta B + \iint_S B \frac{\partial}{\partial n}\left(\frac{1}{r}\right) dS = -\iint_S \mathbf{n} \cdot \frac{\partial(\mathbf{V}_\infty + \mathbf{v})}{\partial t}\left(\frac{1}{r}\right) dS - \iint_S \nu \frac{\mathbf{r} \cdot (\mathbf{n} \times \boldsymbol{\omega})}{r^3} dS + \iiint_V \frac{\mathbf{r} \cdot ((\mathbf{V}_\infty + \mathbf{v}) \times \boldsymbol{\omega})}{r^3} dV$$

The authors used this approach for predicting the fuselage pressure in rotor-fuselage interactions, and discussed the result in Ref. 11. Figure 3 shows the computed pressure distributions with the experiment data (Ref. 18) and the predictions obtained by using the Euler solver (Ref. 10-11).

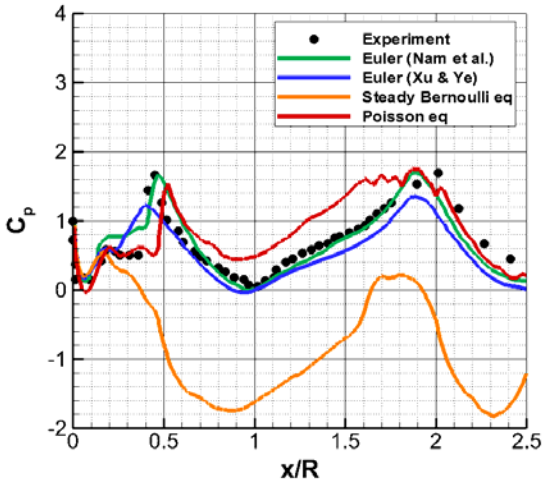

Figure 3 Time-averaged pressure on top of the Georgia Tech fuselage model in forward flight (Ref. 12)

2.1.2. Vortex Dynamics

The velocity of vorticity in the Poisson equation is composed of the velocity of the vorticity in the wake and the velocity due to the fuselage and blades. The vorticity is modelled as vortex particles and the bodies are modelled by the boundary elements on the surface.

2.1.2.1. Vortex Particle Method (VPM)

The vortex particle method developed for rotor flow simulation (Ref. 13) was used to model wake flows in the present research. Initially, the full span wake filaments are convected from the trailing edge of the rotor blade. After 2 or 3 time marching steps, the vortex filaments are split into vortex particles, and convected at the local fluid velocity. The velocity induced by the vortex filament and particle is calculated using the Biot–Savart law incorporated with the vortex core models (Ref. 14, 15) and high-order algebraic smoothing function (Ref. 17). The second-order Runge–Kutta method was used for

time integration of the convection of the vortex filament and particle.

2.1.2.2. Panel / Vortex Lattice Method

The flow excluding the body surface and wake regions is assumed to be incompressible, inviscid, and irrotational. The velocity and the Laplace equation are obtained from the gradient of velocity potential, ϕ and the continuity equation, respectively.

(3) $$\nabla^2\phi = 0$$

If a thin blade is assumed to be a lifting surface, its aerodynamics is calculated by using the vortex lattice method (Ref. 10). If the source term in Eq. (2) is negligible owing to the thin blade and the impermeability boundary condition applies to Eq. (2), then the integral equation for the vortex lattice method is derived as

(4) $$\left\{\int_{blade} \mu \frac{\partial}{\partial n}\left(\frac{1}{r}\right) dS - \mathbf{V}_B + \mathbf{V}_{wake} + \mathbf{V}_{fuselage}\right\} \cdot \mathbf{n} = 0$$

where μ is the advanced ratio and $\mathbf{V}_B$ is the induced velocity of the blade and $\mathbf{V}_{wake}$ and $\mathbf{V}_{fuselage}$ are the velocities induced by the rotor wake and the fuselage, respectively. The first term in Eq. (4) represents the lifting surface. Assuming that a constant-strength doublet panel is equivalent to a closed vortex lattice whose strength is the same as that of the doublet, Eq. (4) represents the linear matrix equation for solving the strength of the vortex lattice.

The fuselage was simulated using the source-doublet panel method, which requires the potential induced by the wake to solve Eq. (2). As the potential cannot be obtained directly from the vortex filament and particles, the boundary integral formulation proposed by Gennaretti (Ref. 12) was used. In this method, the effect of vorticity in the flow field is considered using a source term instead of the potential, as follows:

(5) $$\sigma = \left(\mathbf{V}_F - \mathbf{V}_{blade} - \mathbf{V}_{wake}\right)$$

where $\mathbf{V}_F$ is the fuselage surface velocity and $\mathbf{V}_{blade}$ is the velocity induced by the vortex lattice for the blade. The doublet strength on the fuselage is calculated by using Eq. (2) and (5). The surface pressure on the fuselage is computed using the integral solution of the Poisson equation, which considers the increase in stagnation pressure in the wake flow due to rotor thrust.

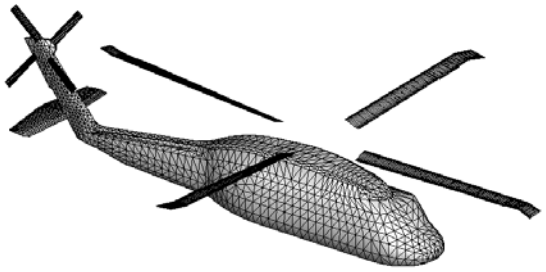

Figure 4 Surface panel mesh for complete UH-60 configuration

2.2. Hover Trim Condition

2.2.1. Analytic Trim with Empirical Formula

2.2.1.1. Trim Equation

A helicopter is said to be in trim in which three forces and moments acting on three orthogonal axes through its center of gravity are in equilibrium.

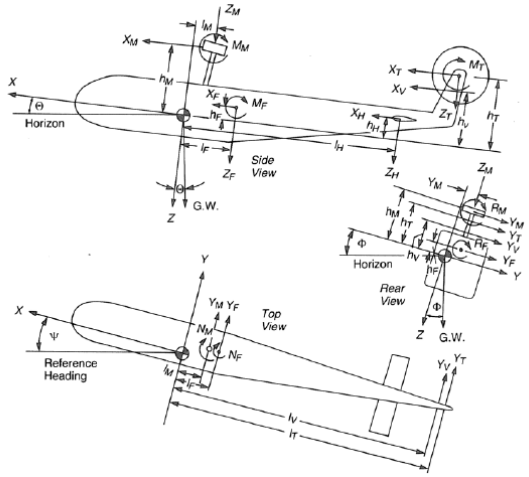

Figure 5 Forces and moments acting on helicopter in trim (Ref. 22)

The aerodynamic forces and moments acting on the helicopter are shown in Figure 5. They are due to the main rotor (M), tail rotor (T), horizontal stabilizer (H), vertical stabilizer (V), and fuselage (F).

The motions the helicopter can experience occur by virtue of the aerodynamic forces and moments. Meanwhile, the system of equations describing the motion can be reduced to six equations that are described by total forces and moments on each of the coordinate axis. These six equations in an equilibrium status, namely, the trim, are as below.

(6)

$$\sum X = 0 \Leftrightarrow X_M + X_T + X_H + X_V + X_F = GW\sin\Theta$$
$$\sum Y = 0 \Leftrightarrow Y_M + Y_T + Y_V + X_F = -GW\sin\Phi$$
$$\sum Z = 0 \Leftrightarrow Z_M + Z_T + Z_H + Z_V + Z_F = -GW\cos\Theta$$
$$\sum R = 0 \Leftrightarrow R_M + Y_M h_M + Z_M y_M + Y_T h_T + Y_V h_V + Y_F h_F + R_F = 0$$
$$\sum M = 0 \Leftrightarrow M_M - X_M h_M + Z_M l_M + M_T - X_T h_T + Z_T l_T - X_H h_H + Z_H l_H - X_V h_V + M_F + Z_F l_F - X_F h_F = 0$$
$$\sum N = 0 \Leftrightarrow N_M - Y_M l_M - Y_T l_T - Y_V l_V + N_F - Y_F l_F = 0$$

They can be treated as two independent sets; the longitudinal (X, Z, and M) and lateral-directional (Y, R, and N) solutions. Each trim solution (longitudinal, and lateral-directional) is written by linear equations for three unknowns and then they can be solved simultaneously.

- Longitudinal trim solution unknown values:

Main rotor thrust (T_M), fuselage pitch attitude (Θ), and longitudinal flapping angle (β_{1c})

- Lateral-directional trim solution unknown values:

Tail rotor thrust (T_T), fuselage roll attitude (Φ), and lateral flapping angle (β_{1s})

The main rotor thrust can be computed by longitudinal trim solution

(7) $$T_M = \frac{GW}{1-\left[\left(\frac{D_{Vertical}}{GW}\right)_H + \left(\frac{D_{Vertical}}{GW}\right)_F\right]}$$

(8) $$C_T = \frac{T_M}{\rho A(\Omega R)^2}$$

Once thrust is obtained, momentum theory is used to find the main rotor torque.

(9) $$Q = C_Q \rho A(\Omega R)^2 R$$

(10) $$C_Q = C_P = C_{P_i} + C_{P_0} = \frac{\kappa C_T^{3/2}}{\sqrt{2}} + \frac{\sigma C_{d_0}}{8}$$

Also, the tail rotor thrust and torque can be calculated such as the main rotor. To consider a non-ideal effect in hover flight, a correction factor (Ref. 25) $\kappa = 1.15$ is applied in induced power calculation. Additionally, mean profile drag coefficient $C_{d_0} = 0.008$ for UH-60A [R4] are used for more accurate profile power calculation. In hover flight, since parasite power which is considerably small compared with induced and profile power, it is currently not considered.

2.2.1.2. Fuselage Vertical Drag Force

In the current research, to consider the vertical drag contributing to the fuselage in hover, the vertical drag ratio is used in trim solutions. The fuselage can divided into segments and the drag coefficient for each segment depends on the shape of cross section. Using the drag coefficient and the dynamic pressure for each segment, the vertical drag ratio can be calculated by summing the product of the drag coefficient and the dynamic pressure ratio, and the projected area of each segment. The vertical drag ratio calculated by Lowry (Ref. 24) for UH-60A fuselage is applied to predict more accurately the trim of the helicopter.

(11) $$\frac{D_V}{GW} = \frac{2\sum_{n=1}^{N} C_{d_n}(q/DL)_n A_n}{A}$$

2.2.1.3. Tail Rotor-Fin Interference in Hover

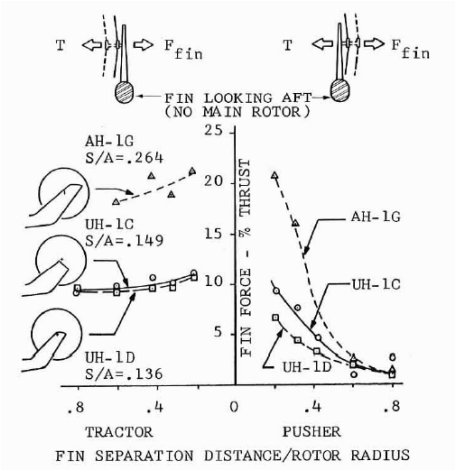

Figure 6 Effect of tail rotor-fin separation (Ref. 26)

An interference of the tail rotor and the vertical fin effect besides fuselage vertical drag is considered for the purpose of estimating the trim precisely. The interference ratio between the tail rotor and the fin can be estimated with a function of the blockage area of them and fin-tail rotor distance as shown in Figure 6 (Ref. 26).

2.2.1.4. Trim Control Angle

The trim control angles such as collective and cyclic pitch angle are computed using the closed-form equations using blade element method. The collective pitch of main rotor is calculated by Eq. (12). Also, the cyclic pitch of the main rotor can be calculated using below Eq. (13) and (14).

- Collective pitch angle

(12) $$\theta_0 = \frac{3}{2}\left(\frac{4}{a}\frac{C_T}{\sigma} - \frac{1}{2}\theta_1 + \frac{1}{\Omega R}\sqrt{\frac{T}{2\rho A}}\right)$$

- Longitudinal cyclic pitch angle

(13) $$\theta_{1s} = -\beta_{1c}$$

- Lateral cyclic pitch angle

(14) $$\theta_{1c} = \beta_{1s}$$

Furthermore, slant angle of tail rotor [R2] is applied to find out accurately collective pitch.

- Tail rotor collective pitch angle

(15) $$\theta_{0,\mathrm{T}} = \frac{3}{2}\left(\frac{4}{a}\frac{C_T}{\sigma} - \frac{1}{2}\theta_1 + \frac{1}{\Omega R}\sqrt{\frac{T}{2\rho A}}\right) - a_0 \tan\delta_3$$

2.2.2. Numerical Trim

Accurate prediction of a hover turn flight is only possible if the perfect hovering is given as an initial condition. Therefore, it is quite important to find the pilot input values to keep the motionless hover flight. A numerical trimming procedure has been generally used for rotors in order to achieve a specified operating condition such as forward flight (Ref. 7-10). The target collective and cyclic pitch angles of the main rotor are obtained through the numerical trim process in order to satisfy the desired thrust of the main rotor and the moments of the system. In the present paper, the authors extend this to the tail rotor, which means that the desired tail rotor thrust value will be also considered to find the target collective pitch angle of the tail rotor and obtain the desired forces and aerodynamic moments.

2.3. Flight Dynamics

2.3.1. Nonlinear Dynamics

The helicopter can perform a hover turn by increasing or decreasing the pitch angle of a tail rotor. The helicopter rotates with transient angular acceleration by the offset of yawing moment generated by the tail rotor. The simplified flight dynamics of the hover turn can be described by using the angular momentum equation as follows.

The non-linear momentum theory based on 6-DOF dynamic equations can be written as follows:

$$\begin{aligned}
F_X &= -T_M(i_M + \beta_{1c}) - GW\Theta = 0 \\
F_Y &= T_M\beta_{1s} + T_T\cos\theta_{cant} + GW\Phi = 0 \\
F_Z &= -T_M - T_T\sin\theta_{cant} + T_M D_{GW} + GW = 0 \\
M_X &= \left(\frac{dR_M}{da_{1_s}}\beta_{1s} + T_M h_M\beta_{1s}\right) - T_M y_M + T_T\cos\theta_{cant} y_T \\
&\quad - T_T\sin\theta_{cant} y_T - D_V h_V = 0 \\
M_Y &= \left(\frac{dM_M}{da_{1_s}}\right)\beta_{1c} + T_M(i_M + \beta_{1c})h_M - T_M l_M \\
&\quad - Q_T + D_F h_M = 0 \\
M_Z &= Q_M - T_T l_T + D_V l_V = I_{zz}\ddot{\Psi}
\end{aligned} \tag{16}$$

where each of Q, T, D, l is the torque, thrust, drag and moment arm of the subscripted components, I_{XX}, I_{YY}, I_{ZZ} are the moment of inertia of the system, and $\ddot{\Psi}$ is the angular acceleration. In a hover condition, Vertical fin drag (D_V) term still exists because of the drag generated from tail rotor wake. The induced velocity due to the tail rotor wake is assumed using far-field uniform flow based on momentum theory ($2v_i$). If all of RHS terms are equal to zero, it becomes a hover flight. However, in fact, there exists the variation in the tail rotor thrust. Accordingly, the helicopter will rotate with an angular acceleration. In this paper, we assume that the Hover turn maneuver is 1 DOF motion, so we only solve 1-DOF equation of motion, yaw motion.

2.3.2. Analytic Model of Aerodynamics with Empirical Formula

In analytic method, momentum theory is one of good tools to calculate the thrust of the rotor. Based on the momentum theory for a linear twisted blade, the thrust coefficient of the rotor with yaw motion can be calculated as follows.

(17)
$$C_{T_{OGE}} = \frac{C_{l_\alpha}}{4}\left[\frac{2}{3}(\theta_{0,T} + a_0\tan\delta_3) - \frac{1}{\Omega R}\left(\frac{v_c}{2} + \sqrt{\left(\frac{v_c}{2}\right)^2 + \frac{T_{OGE}}{2\rho A}}\right)\right]$$
$$T_{IGE} = T_{OGE} f_g$$

Note that subscript IGE is In Ground Effect; OGE is Out of Ground Effect. For UH-60, the tractor-type tail rotor produces the thrust with partial ground effect, thus the thrust of the tail rotor is increased comparing with rotor thrust without ground effect. The thrust increase ratio f_g is used to estimate the thrust produced by the ground effect.

During a hover turn maneuver, the climb rate v_c can be assumed to be $l_T\cos\theta_{cant}\dot{\Psi}$, which means the thrust and drag are non-linear to $\dot{\Psi}$. Based on Eq. (19), in momentum results, we separated the results

by drag modelling. We design the UH-60 fuselage with several cylinders and flat plate as a vertical fin to determine yawing moment due to the drags of the fuselage (F) and the vertical fin (V) generated by yaw movement. To calculate the drag of the fuselage, first, set the C_D of Tail boom with experimental result ($C_D = 1.2$), Second, we use C_D obtained by using unsteady 2-D cylinder calculation data.

2.3.3. Unsteady Viscous Effect

To investigate the effect of unsteady viscous force on the fuselage and the tail boom, URANS (Unsteady Reynolds Averaged Navier-Stokes) calculation was conducted for simplified cross sections in 2D of the fuselage and the tail boom. k-ω SST turbulence model was chosen to capture the transient flow fields of blunt bodies like wakes.

The locations of the sections are sampled at two and three positions from the centre of gravity of a helicopter on the fuselage and the tail boom. An ellipse is used for the section of the fuselage and a circle for the tail boom. Moreover, the cross-section of a vertical stabilizer with another ellipse is considered. The simulations for them are performed increasing linearly the free stream velocity up to the values corresponding Reynolds numbers evaluated. Transient C_d s are computed and normalized by those maximum values for the ellipse and circle sections to compare them each other on the same scale with time. Ellipse (2:1) (the ratio of semi-major and minor axes) is used for the cross-section of the fuselage and ellipse (1:2) for it of a vertical fin as shown in Figure 7.

Figure 7 Three types of configurations for simplified cross-sectional areas of a tail boom, a fuselage, and a vertical fin

It is shown in Figure 8 that unsteady variations of normalized C_d at each case are illustrated and compared. These C_d values will be utilized for the analytic computation for the hover turn so that it can consider the unsteady viscous effect and compare the results with ones of actual flight tests, namely, the angle and the rate of yaw.

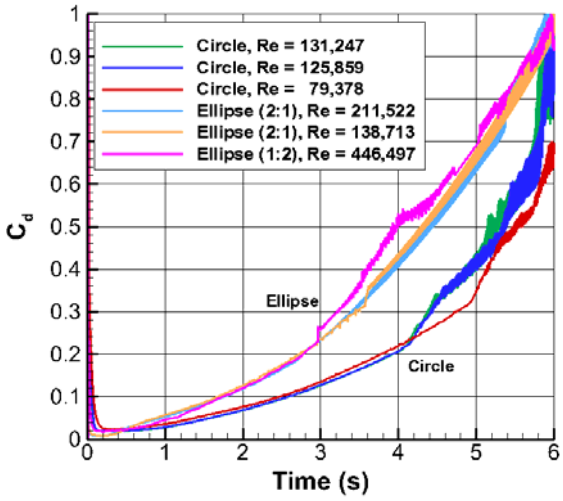

Figure 8 Transient drag coefficients of circular and elliptical sections

The transient fluctuations of C_d s for three configurations are not big until the yaw angle of the fuselage Ψ becomes 100 deg, however, the unsteady fluctuations turn out clear after that and the difference between those behaviours of the circle and the ellipse cross-sections tend to vividly decrease as the hovering turn performs.

An ultimate goal is to construct a look-up table of C_d for several sections on the fuselage and the tail boom in which the unsteady viscous effect can be taken care of without full CFD computations of a complete helicopter and, subsequently, it will be used for our unsteady and inviscid simulation code using vortex particle method for the complete helicopter for the sake of taking into account the unsteady viscous effects.

2.3.4. Dynamic Trim

While we can simplify the hovering turn maneuver in 1 DOF motion, during hover turn maneuver, the trim conditions of other 5-DOF motions are changed simultaneously by time. As the yaw motion (M_Z) is highly dependent on main rotor torque (Q_M), it is necessary to find out the trim conditions at each time step. The 6-DOF equations of motion only with yaw motion can be written as follows.

(18)

$$M_Z = Q_M - T_T l_T + D_V l_V = I_{zz}\ddot{\Psi} \qquad \rightarrow T_T$$

$$F_Z = -T_M - T_T \sin\theta_{cant} + T_M D_{GW} + GW = 0 \qquad \rightarrow T_M$$

$$M_Y = (\frac{dM_M}{da_{1_s}})\beta_{1c} + T_M(i_M + \beta_{1c})h_M - T_M l_M \qquad \rightarrow \beta_{1c}$$

$$-Q_T + D_F h_M = 0$$

$$F_X = -T_M(i_M + \beta_{1c}) - GW\Theta = 0 \qquad \rightarrow \Theta$$

$$M_X = (\frac{dR_M}{da_{1_s}}\beta_{1s} + T_M h_M \beta_{1s}) - T_M y_M + T_T \cos\theta_{cant} y_T$$

$$-T_T \sin\theta_{cant} y_T - D_V h_V = 0 \qquad \rightarrow \beta_{1s}$$

$$F_Y = T_M \beta_{1s} + T_T \cos\theta_{cant} + GW\Phi - \sum D_F = 0 \qquad \rightarrow \Phi$$

In dynamic trim, the 6-DOF equations of motion are calculated sequentially, to calculate each of trim condition that fits for each time step. As the drags of a fuselage and a vertical fin change by time, each of trim conditions calculated from equations above like main rotor torque (Q_M) changes. Based on the results of dynamic trim, yaw angle and yaw rate response will be changed.

3. HOVER TRIM RESULTS

The trim analysis of a full configuration of UH-60A helicopter in hover flight was conducted as a preliminary process before hover turn flight is solved.

3.1. Analytic Trim with Empirical Formula

Once the thrust and the torque of the main and tail rotors are estimated through momentum theory, the analysis of trim can be performed by solving simultaneously the separated longitudinal and lateral-directional trim solutions. The longitudinal flapping angle and the pitch attitude of the helicopter can be attained by a longitudinal trim solution and the lateral flapping angle and the roll attitude of it through a lateral-directional trim solution as well. The result of each trim solution is show in Table 1 as below.

Table 1 Analytic trim results

Longitudinal trim		Lateral-directional trim	
Main rotor thrust	74230.89 N	Tail rotor thrust	6730.89 N
Longitudinal flapping angle	-0.74 deg.	Lateral flapping angle	0.83 deg.
Pitch attitude	6.20 deg.	Roll attitude	-2.11 deg.

3.2. Numerical Simulation

Given the pilot control input obtained from the analytic trim analysis as initial condition, the hovering flight of the UH-60 full configuration was simulated using the vortex lattice/panel/vortex particle method. Here, it is assumed that the helicopter's attitude is fixed without free motion during hover flight. Figure 9 shows the convergence history of z-direction force (thrust) and 3 axis moment. The solution continues fluctuation of small amplitude, but the averaged value seems to converge after 13 rotor revolution time.

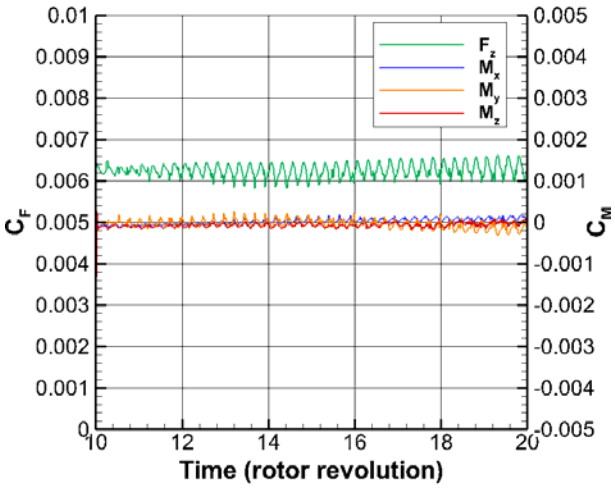

Figure 9 Convergence history of force and moment coefficients

The fuselage surface pressure was computed using the integral solution of the Poisson equation. Figure 10 describes the x-direction location which is the distance from the nose of the fuselage, the time-averaged pressure distribution along the top line of the fuselage is shown in Figure 11. In the region closer to the outboard of the blade, the Poisson approach predicts the pressure coefficient of greater-than-unity, which cannot be captured by the steady Bernoulli equation. The contribution of the blade and wake are also plotted together, which helps understanding of the reason for stagnation pressure increase.

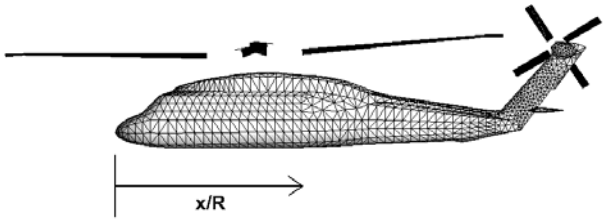

Figure 10 Location for time-averaged surface pressure of the UH-60 fuselage

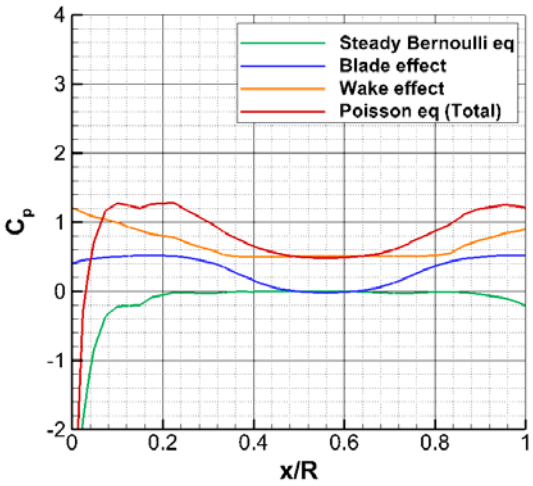

Figure 11 Time-averaged pressure on top of the UH-60 fuselage in hover flight

Time history of the wake structure from 5 to 20 rotor revolution is described in Figure 12. The strength of the wake vortex is described by color and size of the vortex particle. The starting vortex particles resides near the helicopter at the initial stage, and they are convected away to far-field downstream after 15~20 rotor revolutions.

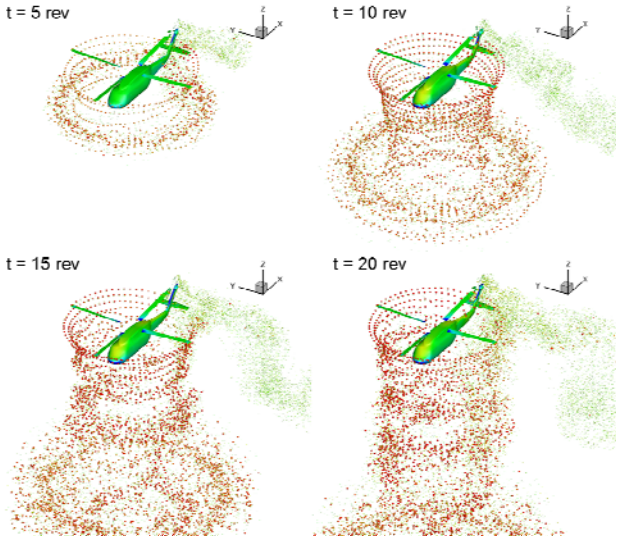

Figure 12 Wake structure in hover flight

3.3. Numerical Trim

Numerical rotor trim is activated after the solution of the hover flight simulation is converged enough. The collective and cyclic pitch angles are adjusted such that the desired z-direction force and zero moments are achieved. Figure 13 and Figure 9 show the time history of the pilot control input and the corresponding aerodynamic loading during the numerical trim procedure. The numerically trimmed pilot control input will be compared with the flight test data as well as analytic trim result in the next chapter.

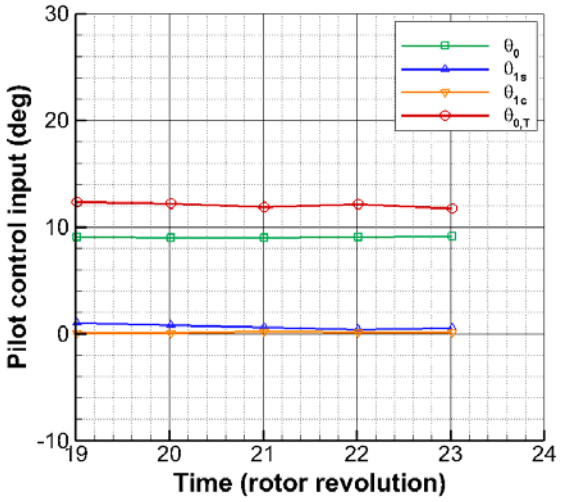

Figure 13 Convergence history of trimmed pilot control inputs

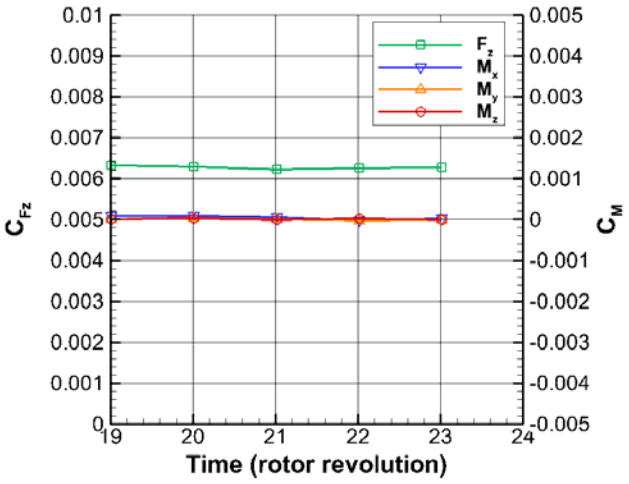

Figure 14 Convergence history of time-averaged force and moment coefficients

3.4. Comparison

Comparison of the trimmed pilot control angle and flight test data is shown in Table 2. The difference in control angle between analytic trim results and flight test data might be caused by structure distortion. In this paper, there might exist the discrepancies with the flight data since structure analysis was not executed. It is identified that the results of the numerical trim are different from the flight test data. The absence of viscous effect in the numerical aerodynamic method applied in the present study can contributes to this discrepancy with the flight test.

Table 2 Comparison of the trim control angle with flight test

	Analytic	Numerical	Flight test

Main rotor collective pitch	9.00	9.12	9.80
Longitudinal cyclic pitch	0.74	0.51	0.09
Lateral cyclic pitch	0.83	0.13	0.77
Tail rotor collective pitch	10.89	11.71	10.36
Pitch attitude	6.20	6.20 (Fixed)	5.00
Roll attitude	-2.11	-2.11 (Fixed)	-2.50

(Unit: deg.)

The difference pilot input between analytic trim results and flight test values might be caused by structure deflection. In this paper, does not conduct structure analysis. Also, numerical trim result has a difference from flight test value. (reason)

4. HOVER TURN SIMULATION

4.1. Analytic model with Empricial Formula

In this paper, to observe the change of yaw angle and yaw rate response by tail rotor input, we compare the non-linear momentum equation to flight test data and GENHEL simulation introduced in Ref. 25. The pedal input introduced in Ref. 25 is converted to tail rotor collective pitch angle using a pedal to tail rotor collective pitch angle ratio introduced in Ref. 28. Each of result with dynamic trim condition and non-dynamic trim condition where main rotor torque Q_M is constant, are compared.

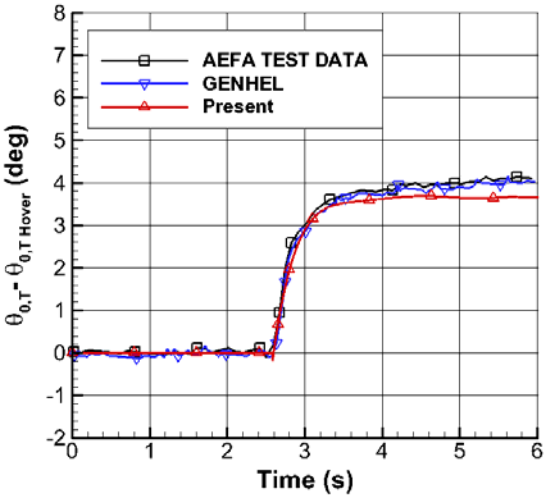

Figure 15 Comparison between pilot input of AEFA Test data, GENHEL and present

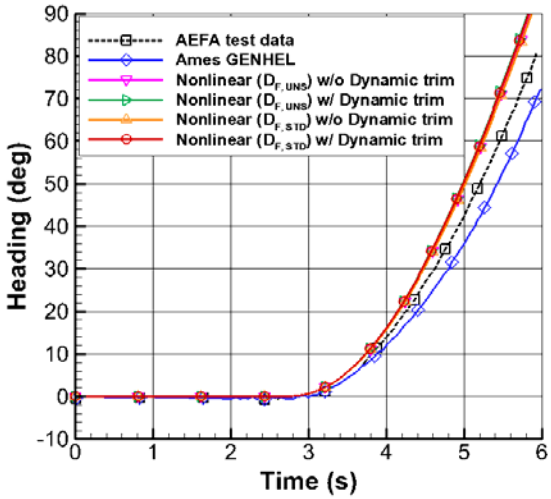

Figure 16 Comparison between Heading angle result of AEFA Test data, GENHEL and Nonlinear Momentum theory with or without Dynamic trim and Unsteady Tail boom drag

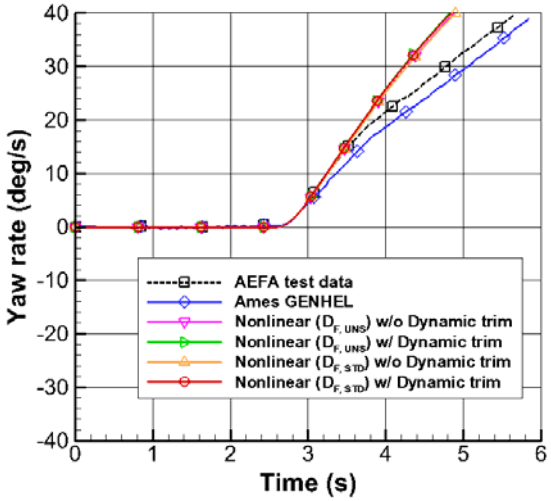

Figure 17 Comparison between Yaw rate ($\dot{\Psi}$) result of AEFA Test data, GENHEL and Nonlinear Momentum theory with or without Dynamic trim and Unsteady Tail boom drag

Note that subscripts STD, UNS means steady and unsteady drag coefficients used.

Figure 15 shows the input tail rotor collective pitch angle. From Figure 16 and Figure 17, we can observe that unlike GENHEL result, which is slightly underestimated with AEFA Test data, momentum results are slightly overestimated. While dynamic trim is calculated as the tail rotor thrust is increased, because of the tail rotor cant angle, the main rotor thrust (T_M) is reduced, which means that main rotor torque (Q_M) is decreased. The result shows that because of the main rotor torque decrement, the yaw rate is shown slightly overestimated than previous non-dynamic trim result. However, with same results based on nonlinear momentum theory

and different Drag modeling (steady or unsteady), the results shows almost no difference.

From Figure 16 and Figure 17, between nonlinear result and test result, some errors are shown. We can predict that the cause of the error is the drag we predict. Because of the difference between uniform tail rotor wake flow and real non-uniform tail rotor wake flow, the prediction of drag produced due to tail rotor wake might be varied. As there are no drag interference models on UH-60 tail rotor cases, here, we test several cases to predict more specifically, yaw angle and yaw rate response (Table 3).

Table 3 Test cases to predict tail rotor wake drag

Case	Property
$D_V = \frac{1}{2}\rho(l_T\ddot{\Psi} + 2v_i + k)^2 S_v C_D$	
Case 1	$D_V = 0$
Case 2	$k = 0$
Case 3	$k = 0.5v_i$
Case 4	$k = v_i$

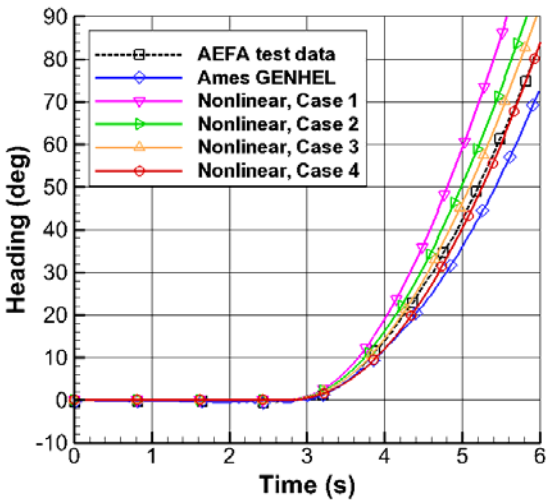

Figure 18 Comparison between heading angle result of AEFA Test data, GENHEL and Nonlinear cases

From Figure 18 and Figure 19, if we estimate the velocity acting on a vertical fin as 3 times larger than induced velocity (v_i), the result predicts well test data for the yaw angle and yaw rate response. It is clear that the non-uniform flow acting on vertical fin should be estimated larger than far-field out of ground condition.

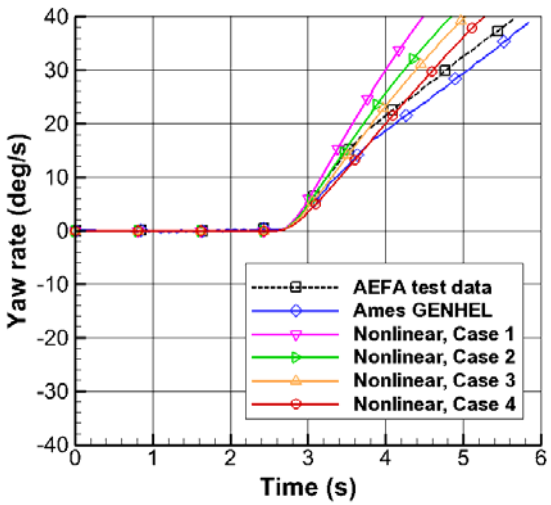

Figure 19 Comparison between Yaw rate ($\dot{\Psi}$) result of AEFA Test data, GENHEL and Nonlinear cases

4.2. Numerical Simulation

The hovering turn was simulated using the coupled aerodynamics-flight dynamics solver. The pedal input of Figure 15 was used here. As mentioned before, the simplified 1 DOF flight dynamics was used for simulating yawing motion.

Figure 20 and Figure 21 show the time history of heading angle and yawing rate during the hover turn, respectively. The computed attitude and yawing rate show similar tendency following the test data. The result is reasonable considering that the present method assumes inviscid flow and uses the simplified 1 DOF yawing-free motion without any dynamic trim. Also, the present solver does not include the structural dynamics, which should be accounted for in the near future.

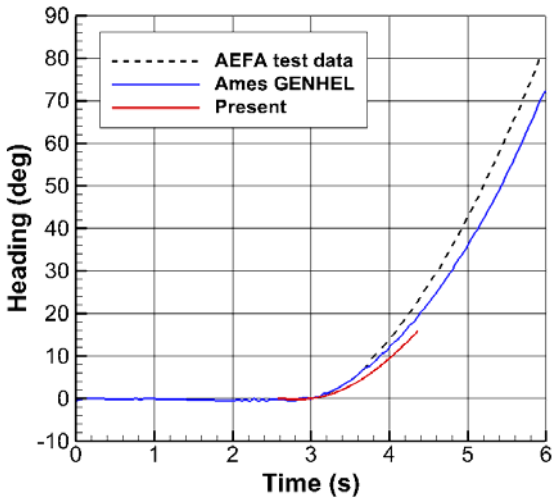

Figure 20 Heading angle comparison with flight-test and Ames GENHEL data

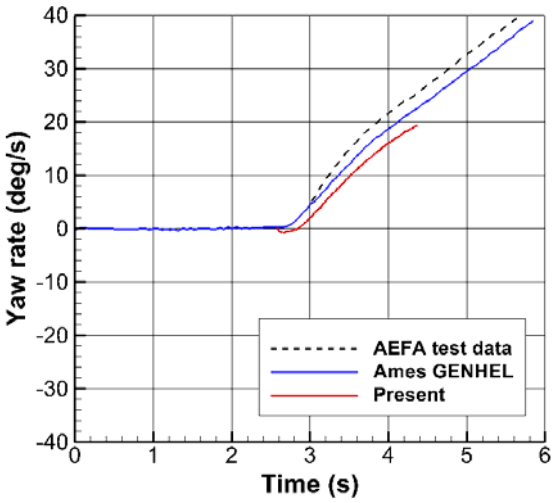

Figure 21 Yaw rate comparison with flight-test and Ames GENHEL data

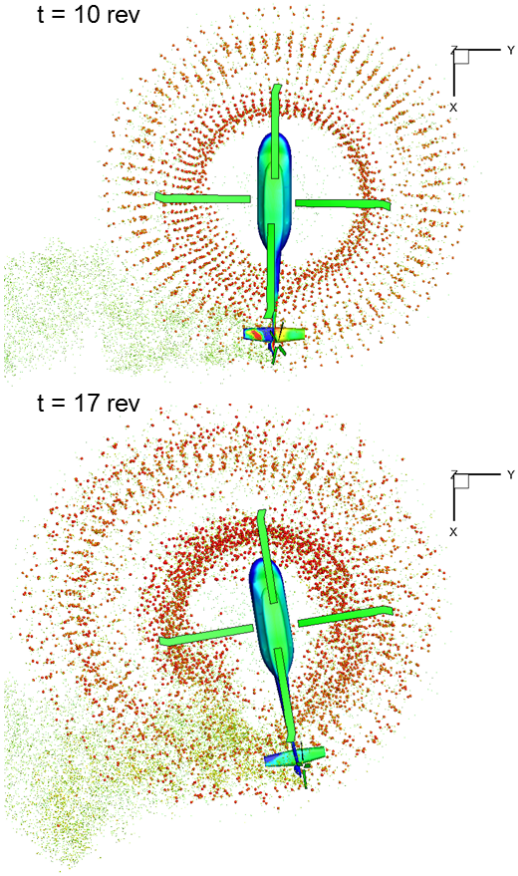

Figure 22 Helicopter heading change and wake geometry during hover turn

4.3. Dynamic Trim Application

To maintain the hovering turn maneuver, the pilot input values should be changed with time. From the Eq. (21), the pilot input values of trim condition to maintain the hover turn maneuver can be calculated analytically.

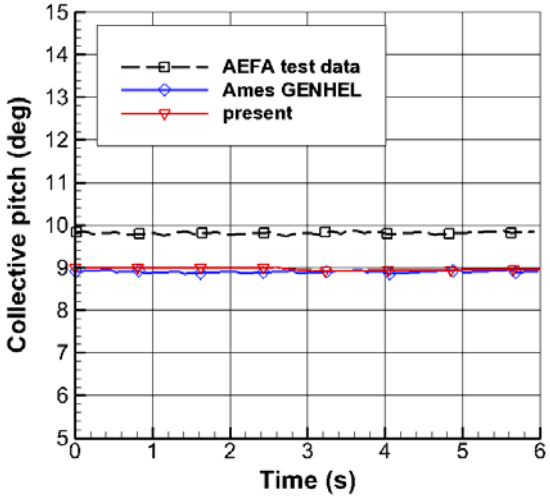

Figure 23 Dynamically trimmed collective pitch angle

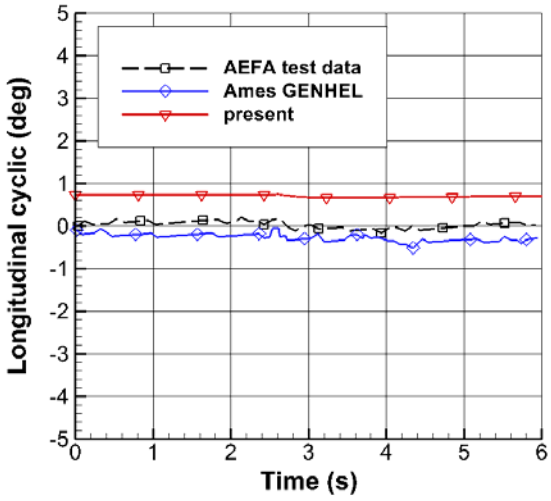

Figure 24 Dynamically trimmed longitudinal cyclic pitch angle

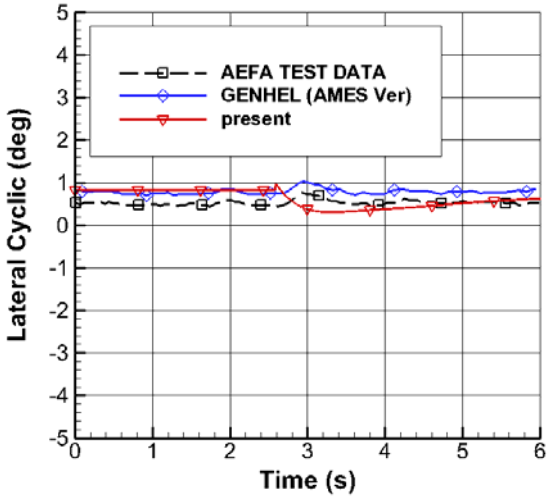

Figure 25 Dynamically trimmed lateral cyclic angle

From Figure 23, Figure 24, based on the analytic method, the pilot input values of main rotor collective pitch (θ_0) and longitudinal cyclic angle (θ_{1s}) follows similar trend with flight test data, with each of less than 1 degree of error. However, in Figure 25, lateral cyclic angle (θ_{1c}) shows initially reversal trend, but follows trend at last. Based on the results, the usage of the analytic trim equation is believed to be a reasonable method for the preliminary procedure to predict pilot inputs during a maneuvering flight.

5. CONCLUSION

Helicopter accident statistics data reveals that the yawing control is one of the important issues for securing safety. As a preliminary research for understanding the loss of tail rotor control effectiveness, the hovering turn flight was chosen for the theme of the analytic and numerical analysis. The present can be summarized as:

- Analytic trim equation for hover flight was solved, and the required pilot control input was obtained through analytic aerodynamics with the empirical correction. The pilot control input angle was used for initial condition of the numerical aerodynamic simulation.
- Aerodynamic simulation of the complete helicopter configuration in hover flight was conducted using the vortex method, and fuselage surface pressure was computed using the integral solution of the Poisson equation. The stagnation pressure increase was captured at the top line of the fuselage, which the steady Bernoulli equation failed to predict.
- Numerical rotor trim procedure was additionally adopted after the convergence of the solution in hover flight. The purpose of the numerical trim is to find the accurate pilot control input angles to keep the hover flight before the hovering-turn free flight. The collective and cyclic pitch of the main rotor and the pedal input were obtained through the numerical trim procedure.
- Nonlinear 1DOF flight dynamics was solved analytically. The vertical/horizontal drag force of the fuselage and the drag force of the vertical tail was estimated using the look-up table. Unsteady viscous effect of the cylinder-shaped body was investigated to see the unsteady effect during transient hovering turn motion.
- Hovering turn was numerically solved using the coupled aerodynamics-flight dynamics solver with the 1DOF yaw free motion assumption. The prediction of the heading angle and yaw rate shows reasonable accuracy although the viscous effect was neglected.

There has been many numerical approaches to solver the hover flight of an isolated rotor or forward flight of the rotor-fuselage configuration. However, it is quite rare to find the hover flight simulation of the complete configuration including the analytic and numerical trim analysis. It is challenging for the simulation researchers because the wake dynamics during the hover flight is more complex than expected, and it takes longer time to reach the converged solution, especially if the time-marching method is used. Interference between the main rotor and the tail rotor as well as interactional aerodynamics between rotor and fuselage should be considered in depth. Hovering turn could be the toughest flight condition for simulation depending on the tail rotor direction and the turning direction.

The authors expect that the incorporation of the steady/unsteady viscous effect using the look-up table or the dynamic rotor trim into the numerical solver could be the next research topic to improve the present solver in the near future.

ACKNOWLEDGEMENT

This work was supported by the Mid-career Researcher Program through an National Research Foundation of Korea (NRF) grant funded by the Korean Ministry of Education, Science, and Technology (MEST) (No. 2012R1A2A2A01046264).

REFERENCES

[1] F. D. Harris, “Introduction to autogyros, helicopters, and other V/STOL aircraft: Volume II,” NASA/SP2012-215959, 2012.

[2] J. Cress, “Short Course on Aerodynamics of Helicopter Accidents,” American Helicopter Society 70th Annual Forum, Montreal, Quebec, Canada, May 19, 2014.

[3] S. Ananthan, and J. G. Leishman, “Helicopter Rotor Wake Dynamics during Simulated Tactical Maneuvers,” American Helicopter Society 60th Annual Forum Proceedings, Baltimore, MA, USA, June 7-10, 2004.

[4] J. Jeon, “A Study on the Main Rotor Wake Configuration during Hovering and Vertical Maneuver Flight,” Master dissertation, KAIST, 2013.

[5] A. Abhishek, A. Datta, and I. Chopra,

"Comprehensive Analysis, Prediction, and Validation of UH-60A Blade Loads in Unsteady Maneuvering Flight," AHS Specialists Conference of the American Helicopter Society, SF, USA, June 23-25, 2008.

[6] A, Abhishek, A, Datta, S. Ananthan, and I. Chopra, "Prediction and Analysis of Main Rotor Loads in a Prescribed Pull-Up Maneuver," Journal of Aircraft, Vol. 47, No. 4, July-August, 2010.

[7] Z. Yang, L. N. Sankar, M. J. Smith, and O. Bauchau, "Recent Improvements to a Hybrid Method for Rotors in Forward Flight," Journal of Aircraft, Vol. 39, No. 5, Nov. 2002, pp. 804-812.

[8] Y. M. Park, H. J. Nam, and O. J. Kwon, "Simulation of Unsteady Rotor-Fuselage Interactions Using Unstructured Adaptive Meshes," Proceedings of the 59th Annual Forum of the American Helicopter Society, May 6-8, 2003.

[9] H. J. Nam, Y. M. Park, and O. J. Kwon, "Simulation of Unsteady Rotor-Fuselage Aerodynamic Interaction Using Unstructured Adaptive Meshes," Journal of the American Helicopter Society, Vol. 51, No. 2, 2006, pp. 141-149.

[10] H. Xu, and Z. Ye, "Euler Calculation of Rotor-Airframe Interaction Based on Unstructured Overset Grids," Journal of Aircraft, Vol. 48, No. 2, 2011, pp. 707-712.

[11] J. S. Jang, "Development of Prediction Method for Body Surface Pressure due to Rotor Wakes by using Poisson Integral Equation," Ph. D dissertation, KAIST, 2013.

[12] J. S. Jang, S. H. Park, and D. J. Lee, "Prediction of fuselage surface pressures in rotor-fuselage interactions using an integral solution of Poisson equation," Journal of the American Helicopter Society, Vol. 59, No. 3, 2014, pp. 0420001

[13] B. S. Lee, M. S. Jung, and O. J. Kwon, "Numerical Investigation of Rotor Downwash Effect on Free-Flight Rockets Launched from a Helicopter," 35th European Rotorcraft Forum, Hamburg, Germany, Sep. 22-25, 2009.

[14] B. S. Lee, J. H. Choi, and O. J. Kwon, "Numerical Simulation of Free-Flight Rockets Air-Launched from a Helicopter," Journal of Aircraft, Vol. 48, No. 5, 2011, pp. 1766-1775.

[15] J. S. Uhlman, "An Integral Equation Formulation of the Equations of Motion of an Incompressible Fluid," Naval Undersea Warfare Center (NUWC) Division Newport Technical Report 11086, July 1992.

[16] K. H. Chung, J. W. Kim, K. W. Ryu, T. K. Lee, and D. J. Lee, "Sound Generation and Radiation from Rotor Tip-Vortex Pairing Phenomenon," AIAA Journal, Vol. 44, No. 6, 2006, pp. 1181-1187.

[17] M. Gennaretti, and G. Bernardini, "Novel Boundary Integral Formulation for Blade-Vortex Interaction Aerodynamics of Helicopter Rotors," AIAA Journal, Vol. 45, No. 6, 2007, pp. 1169-1176.

[18] G. H. Vatistas, V. Kozel, and W. C. Mih, "A Simpler Model for Concentrated Vortices," Experiments in Fluids, Vol. 11, No. 1, 1991, pp. 73-76.

[19] D. J. Lee and L. Roberts, "Interaction of a Turbulent Vortex with a Lifting Surface," AIAA 85-0004, AIAA 23rd Aerospace Sciences Meeting Proceedings, Reno, NV, USA, January 14-17, 1985.

[20] G. Winckelmans and A. Leonard, "Contributions to Vortex Particle Methods for the Computation of Three-Dimensional Incompressible Unsteady Flows," Journal of Computational Physics, Vol. 109, No. 2, 1993, pp. 247-273.

[21] A. G. Brand, H. M. McMahon, and, N. M. Komerath, "Surface Pressure Measurements on a Rotor-Airframe Configuration in Forward Flight," AIAA Journal, Vol. 27, No. 5, May 1989, pp. 569-574.

[22] R. W. Prouty, "Helicopter Performance, Stability, and Control," Krieger Publishing Company, Malabar, Florida, 2005

[23] J. Howlett, "UH-60A BLACK HAWK Engineering Simulation Program: Volume Ⅰ - Mathematical Model," NASA CR-166309, 1989.

[24] D. W. Lowry, M. J. Rich, S. Rivera, and T. W. Sheehy, "Structural Concepts and Aerodynamic Analysis for Low Rader Cross Section Fuselage Configuration," USARTL TR-78-17, AVRADCOM, 1978.

[25] M. G. Ballin, "Validation of a Real-Time Engineering Simulation of the UH-60A Helicopter," NASA/TM 88360, 1987.

[26] R. R. Lynn, F. D. Robinson, N. N. Batra, and J. M. Duhon, "Tail Rotor Design Part 1: Aerodynamics," Journal of American Helicopter Society, Vol. 15, No. 1, 1970, pp. 2-15.

[27] J. A. Franklin, "V/STOL Dynamics, Control, and

Flying Qualities,' NASA/TP-2000-209591, Oct, 2000.

[28] K. B. Hilbert, "A Mathematical Model of the UH-60 Helicopter," NASA Technical Memorandum 85890, USAAVSCOM Technical Memorandum 84-A-2.

[29] B. J. Baskett and L. O. Daniel, "Aeronautical Design Standard Performance Specification Handling Qualities Requirements for Military Rotorcraft," United States Army Aviation and Missile command, March, 2000.

NOMENCLATURE

Subscripts

M	Main rotor
T	Tail rotor
H	Horizontal stabilizer
V	Vertical stabilizer
F	Fuselage

Symbol

Θ	Pitch attitude
Φ	Roll attitude
Ψ	Heading
F_X	Force on X-direction
F_Y	Force on Y-direction
F_Z	Force on Z-direction
M_X	Rolling moment
M_Y	Pitching moment
M_Z	Yawing moment
GW	Gross weight
T	Thrust
Q	Torque
D_V	Vertical fin drag
$D_{Vertical}$	Vertical drag
μ	Advance ratio
i_M	Shaft angle
dM_M / da_{1_s}	Hub pitching moment stiffness
dR_M / db_{1_s}	Hub rolling moment stiffness
DL	Disk loading
q	Dynamic pressure
A	Total segment area
A_n	Segment area
σ	Solidity
ψ	Azimuth angle
β	Flapping angle
a_0	Coning angle
δ_3	Slant angle of tail rotor
β_{1c}	Longitudinal flapping angle
β_{1s}	Lateral flapping angle
θ	Blade pitch angle
θ_0	Collective pitch angle
θ_1	Twist angle
θ_{1c}	Lateral cyclic pitch angle
θ_{1s}	Longitudinal cyclic pitch angle
θ_{cant}	Tail rotor cant angle
f_g	Thrust increase ratio
v_i	Rotor induced velocity
m	Mass
I	Moment of Inertia : $\begin{bmatrix} I_{xx} & 0 & I_{xz} \\ 0 & I_{yy} & 0 \\ I_{xz} & 0 & I_{zz} \end{bmatrix}$

Appendix A. Numerical Rotor Trim

The force and moment coefficients can be expressed as a function of the collective and cyclic pitch angles:

$$\begin{aligned} C_{Fz} &= C_{Fz}(\theta_0, \theta_{1c}, \theta_{1s}, \theta_{0,T}) \\ C_{Mx} &= C_{Mx}(\theta_0, \theta_{1c}, \theta_{1s}, \theta_{0,T}) \\ C_{My} &= C_{My}(\theta_0, \theta_{1c}, \theta_{1s}, \theta_{0,T}) \\ C_{Mz} &= C_{Mz}(\theta_0, \theta_{1c}, \theta_{1s}, \theta_{0,T}) \end{aligned} \quad (19)$$

where C_{Fz} , C_{Mx} , C_{My} ,and C_{Mz} represents the coefficient of force in z-direction, rolling moment, pitching moment, and yawing moment respectively. The equilibrium solution can be obtained by updating the trim angles iteratively using Newton-Raphson method:

(20)

$$\begin{pmatrix} \Delta\theta_0 \\ \Delta\theta_{1c} \\ \Delta\theta_{1s} \\ \Delta\theta_{0,T} \end{pmatrix} = \begin{bmatrix} \frac{\partial C_{Fz}}{\partial\theta_0} & \frac{\partial C_{Mx}}{\partial\theta_0} & \frac{\partial C_{My}}{\partial\theta_0} & \frac{\partial C_{Mz}}{\partial\theta_0} \\ \frac{\partial C_{Fz}}{\partial\theta_{1c}} & \frac{\partial C_{Mx}}{\partial\theta_{1c}} & \frac{\partial C_{My}}{\partial\theta_{1c}} & \frac{\partial C_{Mz}}{\partial\theta_{1c}} \\ \frac{\partial C_{Fz}}{\partial\theta_{1s}} & \frac{\partial C_{Mx}}{\partial\theta_{1s}} & \frac{\partial C_{My}}{\partial\theta_{1s}} & \frac{\partial C_{Mz}}{\partial\theta_{1s}} \\ \frac{\partial C_{Fz}}{\partial\theta_{0,T}} & \frac{\partial C_{Mx}}{\partial\theta_{0,T}} & \frac{\partial C_{My}}{\partial\theta_{0,T}} & \frac{\partial C_{Mz}}{\partial\theta_{0,T}} \end{bmatrix}^{-1} \begin{pmatrix} C_{Fz}{}^{desired} - C_{Fz} \\ C_{Mx}{}^{desired} - C_{Mx} \\ C_{My}{}^{desired} - C_{My} \\ C_{Mz}{}^{desired} - C_{Mz} \end{pmatrix}$$

where C_{Fz} = nondimensional gross weight, and $C_{Mx} = C_{My} = C_{Mz} = 0$ for hovering flight.

Appendix B. Equations of Motion (6 DOF)

The equations of motion for the rigid body are obtained from equilibrium state (trim) about the center-of-gravity. These are expressed non-linear and coupled equations with accelerations, either linear or angular, and combinations of velocities.

(21)

$$X_M + X_T + X_H + X_V + X_F = GW\sin\Theta + \frac{GW}{g}(\dot{u} - vr + wq)$$

$$Y_M + Y_T + Y_V + X_F = -GW\sin\Phi + \frac{GW}{g}(\dot{v} - ur + vp)$$

$$Z_M + Z_T + Z_H + Z_V + Z_F = -GW\cos\Theta + \frac{GW}{g}(\dot{w} - uq + vp)$$

$$R_M + Y_M h_M + Z_M y_M + Y_T h_T + Y_V h_V + Y_F h_F + R_F = I_{xx}\dot{p} - qr(I_{yy} - I_{zz})$$

$$M_M - X_M h_M + Z_M l_M + M_T - X_T h_T + Z_T l_T - X_H h_H + Z_H l_H - X_V h_V + M_F + Z_F l_F - X_F h_F = I_{yy}\dot{q} - pr(I_{zz} - I_{xx})$$

$$N_M - Y_M l_M - Y_T l_T - Y_V l_V + N_F - Y_F l_F = I_{zz}\dot{r} - pq(I_{xx} - I_{yy})$$

Appendix C. Pop-up Flight

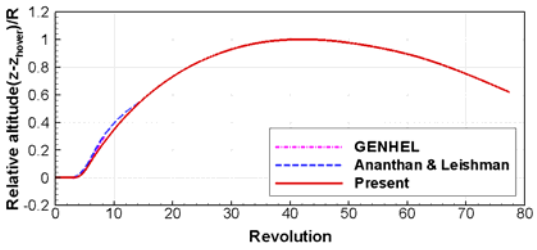

Figure 26 Time history of the relative altitude during pop-up flight

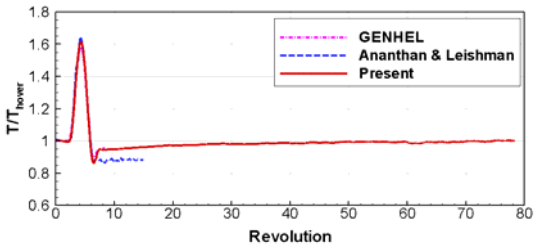

Figure 27 Time history of thrust ratio during pop-up flight

For the purpose of the validation of aerodynamic-dynamic coupling analysis using vortex lattice method and freewake method, pop-up maneuver flight is simulated and compared with other results [Ref. 3]. To understand aerodynamic and dynamic characteristics during pop-up maneuver flight, thrust and altitude are computed near 80 revolutions. It is shown that the time-history results of thrust and altitude are similar them.

Appendix D. UH-60A Helicopter Parameter

Table C.1 UH-60A Helicopter input parameter [R2]

Description	Value	Unit
Gross weight	74009.15	N
Main rotor		
Radius	8.17	m
Rotational speed	27.02	rad/s
Solidity	0.085	-
Twist angle	-0.314	rad
Hinge offset ratio	0.047	-
Lock number	8.1936	-
Shaft angle	-0.05236	rad
Tail rotor		
Radius	1.67	m
Rotational speed	124.55	rad/s
Solidity	0.188	-
Twist angle	-0.314	rad
Moment arm		
h_M	2.28	m
l_M	-0.14	m
y_M	0	m
h_T	1.82	m
l_T	11.27	m
l_F	-0.15	m